

Strain-engineered magnetic order in $(\text{LaMnO}_3)_n/(\text{SrMnO}_3)_{2n}$ superlattices

^{1,2,3}Qinfang Zhang,* ⁴Shuai Dong, ¹Baolin Wang, and ^{2,3,5}Seiji Yunoki

¹Key Laboratory for Advanced Technology in Environmental Protection of Jiangsu Province,
Yancheng Institute of Technology, Yancheng 224051, China

²Computational Condensed Matter Physics Laboratory, RIKEN ASI, Wako, Saitama 351-0198, Japan

³CREST, Japan Science and Technology Agency, Kawaguchi, Saitama 332-0012, Japan

⁴Department of Physics, Southeast University, Nanjing 211189, China

⁵Computational Materials Science Research Team, RIKEN AICS, Kobe, Hyogo 650-0047, Japan

(Dated: October 15, 2018)

Using first-principles calculations based on the density functional theory, we show a strong strain dependence of magnetic order in $(\text{LaMnO}_3)_n/(\text{SrMnO}_3)_{2n}$ (001) superlattices with $n = 1, 2$. The epitaxial strain lifts the degeneracy of Mn e_g orbitals, thus inducing an inherent orbital order, which in turn strongly affects the ferromagnetic double exchange of itinerant e_g electrons, competing with the antiferromagnetic superexchange of localized t_{2g} electrons. For the case of tensile strain induced by SrTiO_3 (001) substrate, we find that the ground state is A-type antiferromagnetic and $d_{x^2-y^2}$ orbital ordered, which is in excellent agreement with recent experiments [S. J. May *et al.*, *Nature Materials* **8**, 892 (2009)]. Instead, for the case of compressive strain induced by LaAlO_3 (001) substrate, we predict that the ground state is C-type antiferromagnetic and $d_{3z^2-r^2}$ orbital ordered.

PACS numbers: 75.70.Cn, 71.20.Be, 75.47.Lx, 75.25.Dk

I. INTRODUCTION

Transition metal oxides in perovskite based structures exhibit a wide variety of phases with different electronic, magnetic, and orbital structures, and show rich functionalities such as high- T_C superconductivity, colossal magnetoresistance, and multiferroics.¹ A recent advance in epitaxial growth techniques has made it even possible to fabricate transition metal oxide heterostructures with sharp and smooth interfaces controlled at the atomic scale.² In these heterostructures, many unique properties, not found in the corresponding alloy compounds made of the same composite elements, have been observed, which include e.g., two dimensional electron gas with high mobility at the heterostructure interfaces,³ indicating the promising potential of oxide heterostructures for future technological applications.⁴

In the case of manganites,⁵ LaMnO_3 is an A-type antiferromagnetic insulator and SrMnO_3 is a G-type antiferromagnetic insulator. On one hand, the randomly-cation-doped alloy $\text{La}_{1-x}\text{Sr}_x\text{MnO}_3$ exhibits a rich magnetic phase diagram, depending on the doping concentration x . On the other hand, La/Sr cation-ordered analogues forming superlattices behave quite differently from their alloy compounds.⁶⁻¹⁰ For example, $\text{La}_{2/3}\text{Sr}_{1/3}\text{MnO}_3$ alloy has a mixed valence of $\text{Mn}^{3+}/\text{Mn}^{4+}$, and the ground state is ferromagnetic half metallic due to the double exchange mechanism.⁵ To the contrary, it is found experimentally that cation-ordered $(\text{LaMnO}_3)_{2n}/(\text{SrMnO}_3)_n$ (001) superlattices are insulating when n is larger than 3.^{6,8} This change of behavior is easily understood because the number n of SrMnO_3 layers control the quantum confinement potential: when n is small, the confinement potential is small and the e_g electrons are distributed uniformly, thus expecting the phases similar to the alloy $\text{La}_{1-x}\text{Sr}_x\text{MnO}_3$. When n is

large, the confinement potential becomes large enough to trap the e_g electrons in LaMnO_3 layers, and thus the bulk properties of LaMnO_3 and SrMnO_3 would be observed. Several theoretical studies for $(\text{LaMnO}_3)_{2n}/(\text{SrMnO}_3)_n$ superlattices have been reported to understand their electronic and magnetic properties.^{11,12}

More recently, Bhattacharya *et al.*^{13,14} have experimentally studied the transport and the magnetic properties of similar superlattices $(\text{LaMnO}_3)_n/(\text{SrMnO}_3)_{2n}$ grown on SrTiO_3 (001) substrate. They have found that the ground state of these superlattices with $n = 1, 2$ are A-type antiferromagnetic metals with Néel temperature (T_N) which is higher than that observed in any alloy $\text{La}_{1-x}\text{Sr}_x\text{MnO}_3$ compound.¹⁴ Although the similar physical principles found in $(\text{LaMnO}_3)_{2n}/(\text{SrMnO}_3)_n$ superlattices are certainly expected to apply here, the systematic theoretical investigations are required to understand the main ingredients which determine the electronic as well as the magnetic properties of $(\text{LaMnO}_3)_n/(\text{SrMnO}_3)_{2n}$ superlattices.

Here, in this paper, performing first-principles calculations based on the density functional theory, we study the electronic and the magnetic structures of $(\text{LaMnO}_3)_n/(\text{SrMnO}_3)_{2n}$ (001) superlattices with $n = 1, 2$. We show that the magnetic properties are governed not only by the quantum confinement potential caused by periodic alignment of cation ions $\text{La}^{3+}/\text{Sr}^{2+}$ but also by the strain induced by substrates on which the superlattices are grown. Namely, for the case of tensile strain induced by SrTiO_3 (STO) (001) substrate, our calculations show that the ground state of these superlattices are A-type antiferromagnetic and $d_{x^2-y^2}$ orbital ordered with higher T_N for $n = 1$ than for $n = 2$. This is indeed in excellent agreement with recent experimental observations.¹⁴ Instead, for the case of compressive strain induced by LaAlO_3 (LAO) (001) substrate, we predict C-

type antiferromagnetic and $d_{3z^2-r^2}$ orbital orders with higher T_N for $n = 1$ than for $n = 2$.

The rest of this paper is organized as follows. After describing the computational details in Sec. II, the numerical results for the cases of SrTiO₃ substrate and LaAlO₃ substrate are presented in Sec. III A and Sec. III B, respectively, followed by discussion of the confinement potential in Sec. III C. Sec. IV summarizes this paper.

II. COMPUTATIONAL METHODS

We perform the first-principles electronic structure calculations based on the projected augmented wave pseudopotentials using the Vienna Ab initio Simulation Package (VASP).^{15,16} The valence states include 3p4s3d and 2s2p for Mn and O, respectively. The electron interactions are described using the generalized gradient approximation (GGA) and the rotationally invariant GGA+ U method^{17–19} with the effective U_{eff} , i.e., $U - J$, from 1 eV to 5 eV for d electron states. Compared to the GGA, the GGA+ U approach gives an improved description of d electron localization.²⁰ The atomic positions of superlattices are fully optimized iteratively until the Hellman-Feynman forces are 0.01 eV/Å or less. The plane-wave cutoff is set to be 500 eV and a $12 \times 12 \times 12$ Monkhorst-Pack k-point grid is used in combination with the tetrahedron method.²¹

The supercells considered here consist of 6 MnO₂ layers, 2 LaO layers, and 4 SrO layers for both $n = 1$ and 2, as shown in Fig. 1 (a) and Fig. 2 (a). We consider 12 and 10 different magnetic moment alignments to search for the ground state magnetic structures for LaMnO₃/(SrMnO₃)₂ and (LaMnO₃)₂/(SrMnO₃)₄ superlattices, as shown in Fig. 3 and Fig. 4, respectively. These magnetic structures include not only simple ferromagnetic, A-type, C-type, and G-type antiferromagnetic structures²² but also magnetic structures with mixed combinations of these simple magnetic structures. The epitaxial constraint on these superlattices, which is grown on substrates, is to fix the in-plane lattice constants. Thus, to simulate the strain effect, we fix the in-plane lattice constants (a) of the superlattices to the ones of substrates, i.e., $a = 3.905$ Å for SrTiO₃ substrate²³ and $a = 3.81$ Å for LaAlO₃ substrate,²⁴ and the lattice constant (c) perpendicular to MnO₂ layers is fully relaxed. Atomic positions are also fully optimized.

III. RESULTS

A. (LaMnO₃)_n/(SrMnO₃)_{2n} on SrTiO₃

Let us first examine (LaMnO₃)_n/(SrMnO₃)_{2n} (001) superlattices on SrTiO₃ (001) substrate. Our systematic GGA calculations reveal that the ground states of these superlattices with $n = 1$ and 2 are both A-type antiferromagnetic metals. A schematic spin alignment

of A-type antiferromagnetic order is shown in Fig. 3 (g) and Fig. 4 (a). Indeed, as shown in Fig. 1 (d) and Fig. 2 (d), the projected spin density distribution, calculated by integrating spin density of occupied states from Fermi level down to -0.5 eV, clearly indicates the A-type antiferromagnetic spin order. Our GGA+ U calculations also find that these A-type antiferromagnetic states are robust against electron correlations, and they are indeed stable up to $U_{\text{eff}} = 2$ eV for $n = 1$ and $U_{\text{eff}} = 1.3$ eV for $n = 2$ (see Fig. 5).²⁵

Since the supercell sizes and the numbers of each type of atoms are the same, we can simply compare the total energy of these two different superlattices. Tab. I summarizes the total energies for the A-type antiferromagnetic states and other magnetic states. Since the A-type (C-type) magnetic structure is ferromagnetic (antiferromagnetic) within the ab plane and antiferromagnetic (ferromagnetic) along the c direction, we can approximately estimate an effective magnetic exchange (J_{eff}) simply by comparing the total energy of the A-type and the C-type antiferromagnetic states. It is clearly observed in Tab. I that the stabilization energy of the A-type antiferromagnetic state, i.e., J_{eff} , is larger for $n = 1$ than for $n = 2$. This implies that T_N for $n = 1$ is higher than that for $n = 2$. These results are in excellent agreement with experimental observations by May *et al.*¹⁴

TABLE I. Total energies (in unit of eV) of (LaMnO₃)_n/(SrMnO₃)_{2n} superlattices ($n = 1, 2$) calculated using GGA. FM, A-AFM, and C-AFM stand for ferromagnetic, A-type antiferromagnetic, and C-type antiferromagnetic states, respectively.

n	SrTiO ₃ substrate			LaAlO ₃ substrate		
	FM	A-AFM	C-AFM	FM	A-AFM	C-AFM
$n=1$	-466.262	-466.636	-465.854	-465.852	-465.459	-466.466
$n=2$	-465.637	-465.885	-465.151	-465.398	-465.015	-465.858

Since the epitaxial constraint of substrates is to fix the in-plane lattice constant a of the superlattices, the tetragonal distortion should inevitably occur, which in turn affects the relative occupation of Mn e_g electrons. Indeed, as shown in Tab. II, we find that the SrTiO₃ substrate induces tensile strain with $a > c$, in which $d_{x^2-y^2}$ orbital is lower in energy than $d_{3z^2-r^2}$ orbital. This can be seen in the projected charge density distribution, the integrated charge density from Fermi level down to -0.5 eV, shown in Fig. 1 (b) and Fig. 2 (b), indicating that e_g electrons preferably occupy $d_{x^2-y^2}$ orbital. Because of this orbital order induced inherently by the substrate strain, the A-type antiferromagnetic order is stabilized. Remember that the magnetic interaction between Mn ions is determined by competition between the ferromagnetic double exchange via itinerant Mn e_g electrons and the antiferromagnetic superexchange between localized Mn t_{2g} electrons. When $d_{x^2-y^2}$ orbital is occupied rather than $d_{3z^2-r^2}$ orbital, the strong double exchange induces ferromagnetic order in the ab plane while the weak itinerancy of $d_{x^2-y^2}$ electrons along the c

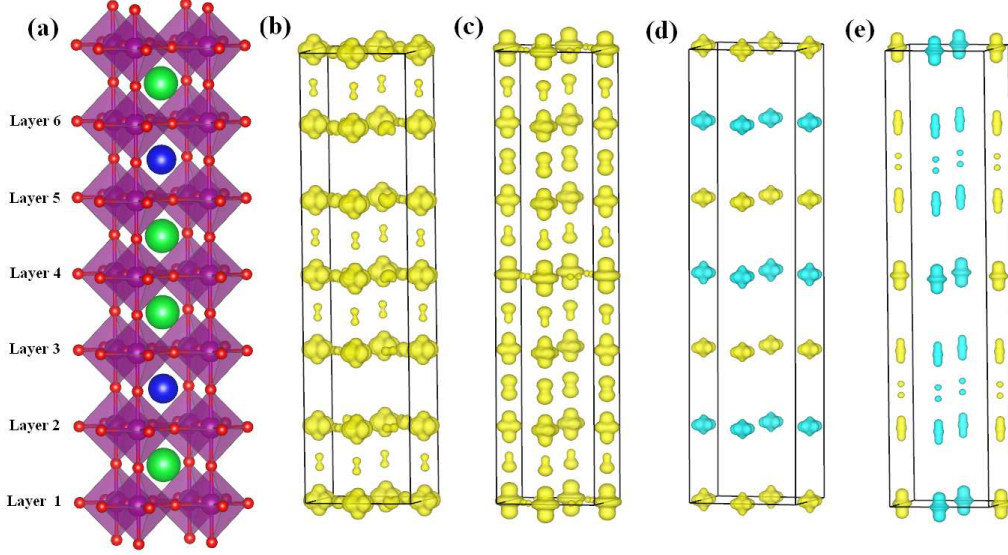


FIG. 1. (Color online). (a) A schematic figure of the supercell considered for $\text{LaMnO}_3/(\text{SrMnO}_3)_2$ (001) superlattices, and the projected charge [(b) and (c)] and spin [(d) and (e)] density distributions (integrated from Fermi level down to -0.5 eV using GGA) for $\text{LaMnO}_3/(\text{SrMnO}_3)_2$ superlattices grown on SrTiO_3 [(b) and (d)] and LaAlO_3 [(c) and (e)] (001) substrates. The loci of MnO layers are indicated in (a), where red, blue, green, and purple spheres indicate O, La, Sr, and Mn atoms, respectively. In (d) and (e), the up and down spin densities are denoted by yellow and light blue, respectively.

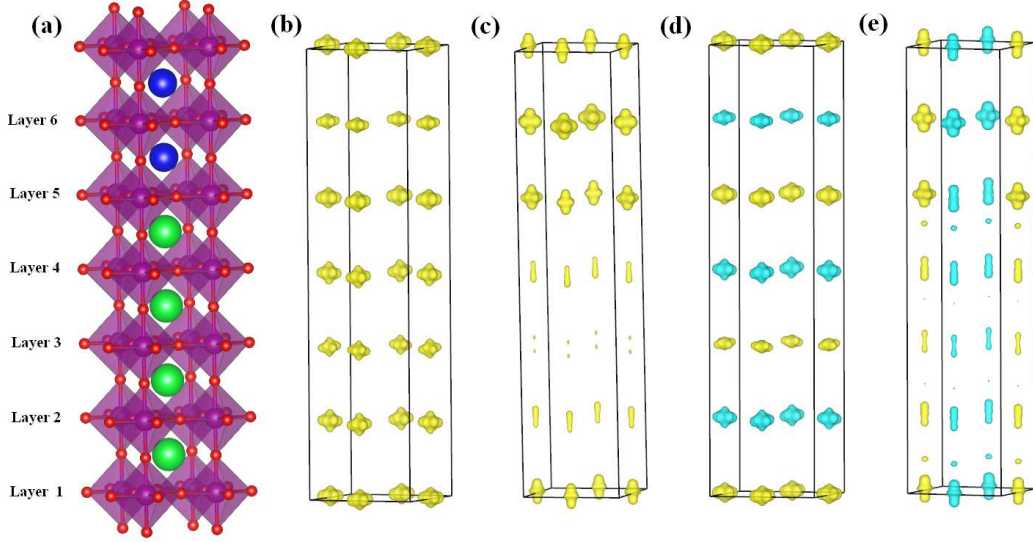


FIG. 2. (Color online). (a) A schematic figure of the supercell considered for $(\text{LaMnO}_3)_2/(\text{SrMnO}_3)_4$ (001) superlattices, and the projected charge [(b) and (c)] and spin [(d) and (e)] density distributions (integrated from Fermi level down to -0.5 eV using GGA) for $(\text{LaMnO}_3)_2/(\text{SrMnO}_3)_4$ superlattices grown on SrTiO_3 [(b) and (d)] and LaAlO_3 [(c) and (e)] (001) substrates. The loci of MnO layers are indicated in (a), where red, blue, green, and purple spheres indicate O, La, Sr, and Mn atoms, respectively. In (d) and (e), the up and down spin densities are denoted by yellow and light blue, respectively.

direction reduces substantially the double exchange and as a result the superexchange between t_{2g} electrons stabilizes antiferromagnetic order along this direction. Finally, it is also interesting to note that the optimized lattice constant c for $n = 1$ is shorter than that for $n = 2$

(see Tab. II), which is also qualitatively in good agreement with experimental observations.¹⁴

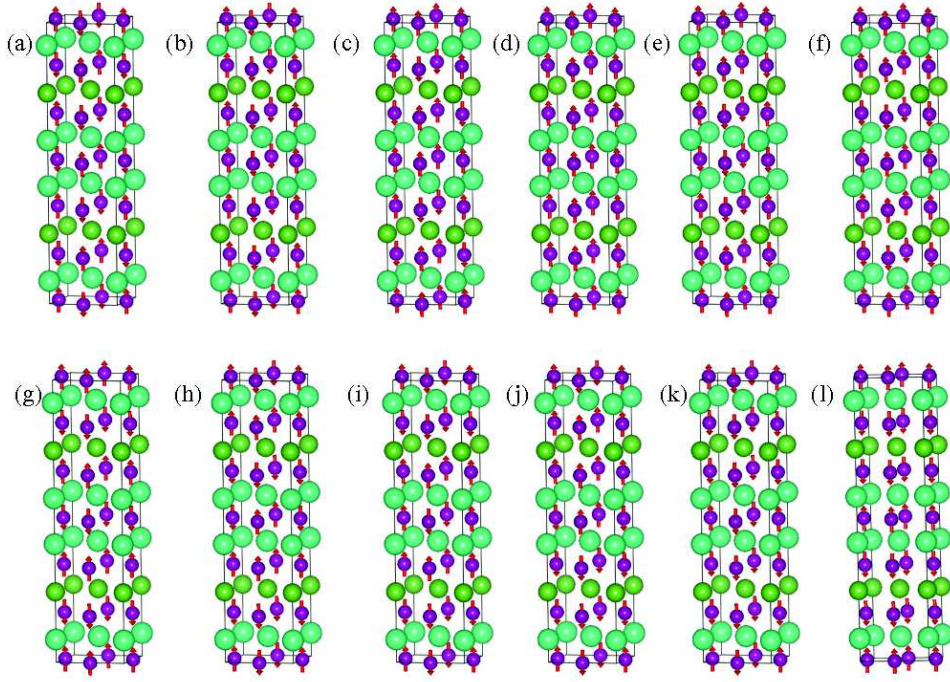


FIG. 3. (Color online). 12 different magnetic structures considered for $\text{LaMnO}_3/(\text{SrMnO}_3)_2$ superlattices: G-AFM (a), C-AFM (b), M1-AFM (c), FM (d), M2-AFM (e), D-AFM (f), A-AFM (g), M3-AFM (h), M4-AFM (i), M5-AFM (j), M6-AFM (k), and D1-AFM (l). Mn spins are indicated by arrows. Aqua, lime, and violet spheres stand for Sr, La, and Mn atoms, respectively. O atoms are omitted for clarity.

TABLE II. The optimized lattice constant c (averaged value within the supercell and in unit of Å) and c/a of $(\text{LaMnO}_3)_n/(\text{SrMnO}_3)_{2n}$ superlattices ($n = 1, 2$) calculated using GGA. The magnetic structures are A-type and C-type antiferromagnetic for SrTiO_3 and LaAlO_3 substrates, respectively.

n	SrTiO ₃ substrate		LaAlO ₃ substrate	
	c	c/a	c	c/a
$n=1$	3.806	0.9746	4.006	1.0115
$n=2$	3.825	0.9795	4.010	1.0525

B. $(\text{LaMnO}_3)_n/(\text{SrMnO}_3)_{2n}$ on LaAlO_3

Now, let us study the electronic and the magnetic properties of $(\text{LaMnO}_3)_n/(\text{SrMnO}_3)_{2n}$ superlattices ($n = 1, 2$) on (001) LaAlO_3 substrate. In the alloy manganites $\text{La}_{1-x}\text{Sr}_x\text{MnO}_3$, it is known that c/a is a key parameter in determining the magnetic ground states.²⁶ Here, we demonstrate that even in these superlattices the magnetic structure can be controlled by the substrate strain which varies c/a .

Because the in-plane lattice constant of LaAlO_3 is much smaller than that of LaMnO_3 (bulk lattice parameter is 3.935Å), it is expected that the LaAlO_3 substrate induces compressive strain. In fact, we find in Tab. II that the lattice constant c in the superlattices is larger

than the in-plane lattice constant a . As a result of this tetragonal distortion, Mn e_g orbitals are split and $d_{3z^2-r^2}$ orbital is lower in energy than $d_{x^2-y^2}$ orbital, which thus induces $d_{3z^2-r^2}$ orbital order. A signature of this orbital order can be seen in the projected charge density distributions shown in Fig. 1 (c) and Fig. 2 (c). Because of this orbital order, the magnetic ground state is expected to be C-type antiferromagnetic. Considering 10 – 12 different candidates for possible magnetic structures as shown in Figs. 3 and 4, our GGA calculations find that the ground states for $n = 1$ and 2 are both C-type antiferromagnetic metals [Fig. 3 (b) and Fig. 4 (b)]. This magnetic alignment can be indeed clearly seen in the projected spin density distribution as shown in Fig. 1 (e) and Fig. 2 (e). It is also interesting to note that the lattice distortion along the c direction is less pronounced for the case of LaAlO_3 substrate as compared to the case of SrTiO_3 substrate. As shown in Fig. 6, Mn-O-Mn angles between the nearest layers along the c direction for the superlattices on LaAlO_3 substrate is almost 180° , which certainly favors the ferromagnetic double exchange along this direction. We also find that the C-type magnetic structure is robust against electron correlations in Mn d orbitals up to $U_{\text{eff}} = 4$ eV for $n = 1$ and $U_{\text{eff}} = 1.5$ eV for $n = 2$ (see Fig. 7).²⁵

As in the case of SrTiO_3 substrate, we can discuss the Néel temperature T_N for the C-type antiferromagnetic

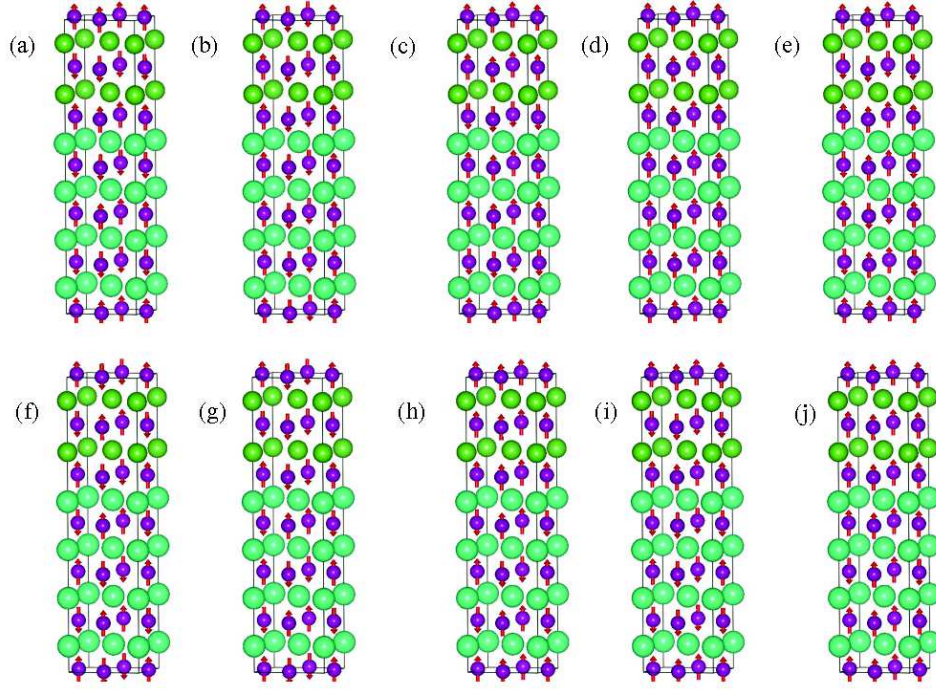


FIG. 4. (Color online). 10 different magnetic structures considered for $(\text{LaMnO}_3)_2/(\text{SrMnO}_3)_4$ superlattices: A-AFM (a), C-AFM (b), D-AFM (c), FM (d), M2-AFM (e), G-AFM (f), M1-AFM (g), M3-AFM (h), M4-AFM (i), and M5-AFM (j). Mn spins are indicated by arrows. Aqua, lime, and violet spheres stand for Sr, La, and Mn atoms, respectively. O atoms are omitted for clarity.

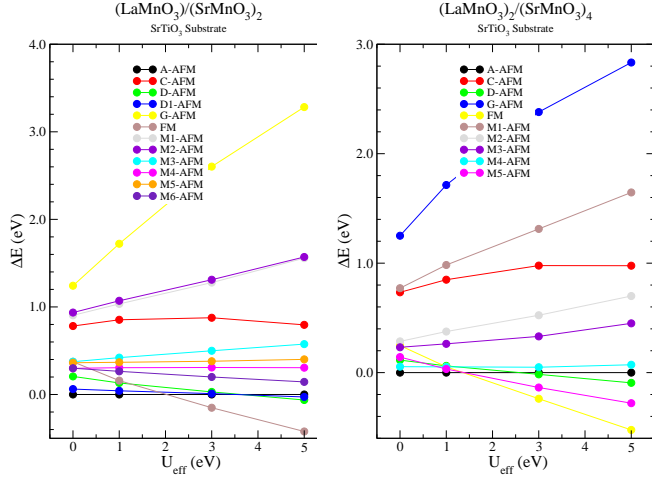


FIG. 5. (Color online). U_{eff} dependence of the relative energies (calculated using GGA+ U) for various magnetic structures (see Fig. 3 and Fig. 4) compared to A-type antiferromagnetic state for $(\text{LaMnO}_3)_n/(\text{SrMnO}_3)_{2n}$ with $n = 1$ (left) and $n = 2$ (right) on SrTiO_3 substrate.

order by calculating the total energy, and the results are summarized in Tab. I. Simply by comparing the total energies of the C-type and the A-type antiferromagnetic

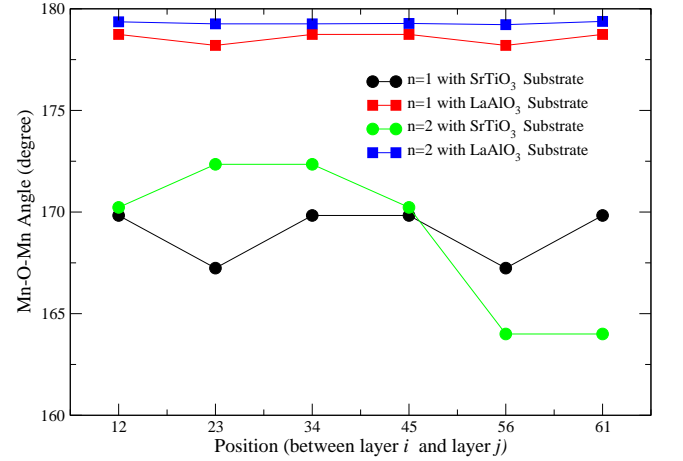


FIG. 6. (Color online). Mn-O-Mn angles between the nearest layers along the c direction for the relaxed crystal structures (calculated using GGA) for $(\text{LaMnO}_3)_n/(\text{SrMnO}_3)_{2n}$ (001) superlattices grown on different substrates indicated in the figure. The layer positions in the horizontal axis are indicated in Fig. 1 (a) and Fig. 2 (a).

states, the difference of which gives a rough estimate of an effective magnetic exchange J_{eff} , we find that the stabilization energy of the C-type antiferromagnetic state,

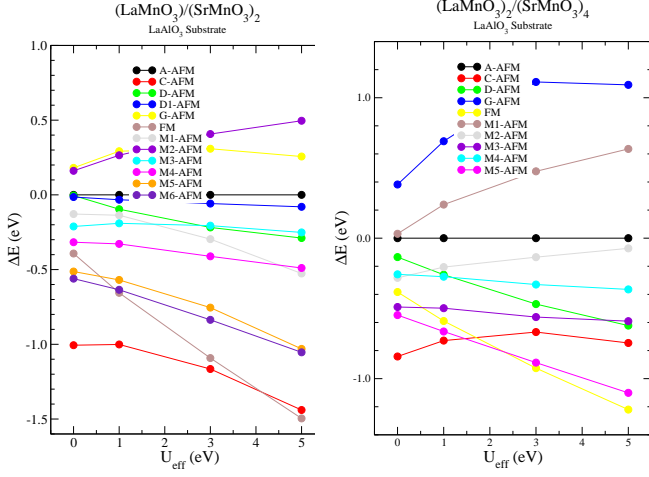


FIG. 7. (Color online). U_{eff} dependence of the relative energies (calculated using GGA+ U) for various magnetic structures (see Fig. 3 and Fig. 4) compared to A-type antiferromagnetic state for $(\text{LaMnO}_3)_n/(\text{SrMnO}_3)_{2n}$ with $n = 1$ (left) and $n = 2$ (right) on LaAlO_3 substrate.

i.e., J_{eff} , is larger for $n = 1$ than for $n = 2$. This implies that T_N for $n = 1$ is higher than that for $n = 2$. Since $(\text{LaMnO}_3)_n/(\text{SrMnO}_3)_{2n}$ superlattices ($n = 1, 2$) on (001) LaAlO_3 substrate have not been studied experimentally, these results provide the theoretical prediction which should be tested experimentally in the future.

C. Confinement potential

Finally, let us briefly discuss why the magnetic and orbital ground states found here are spatially uniform, in spite of apparent periodic potential modulation caused by different ionic charges, i. e., La^{3+} in LaMnO_3 layers, and Sr^{2+} in SrMnO_3 . As reported in Ref. 12, one way to estimate the effective potential modulation is to evaluate the oxygen $1s$ core energy level. The results for $(\text{LaMnO}_3)_n/(\text{SrMnO}_3)_{2n}$ superlattices with $n = 1$ and 2 are shown in Fig. 8. From these figures, we see that (i) the potentials are almost the same for both substrates, and (ii) as is expected, the confinement potential becomes larger with n . The calculated charge density shows that e_g electrons in LaMnO_3 layers is ~ 0.2 (0.1) more than that in SrMnO_3 layers for $n = 2$ ($n = 1$). This suggests that the thickness is still thin enough not to confine e_g electrons in LaMnO_3 layers. However, we naturally expect that the bulk properties may recover far away from interface when n is increased further and a metal-insulator transition should eventually occur.

It is also found that the confinement potential can be more easily estimated simply by calculating Madelung potential. As shown in Fig. 9, Madelung potential can indeed semi-qualitatively reproduce the values estimated from oxygen $1s$ core energy level. This finding should

be very useful in estimating the confinement potential for more complex superlattices in which first-principles electronic structure calculations are computationally ex-

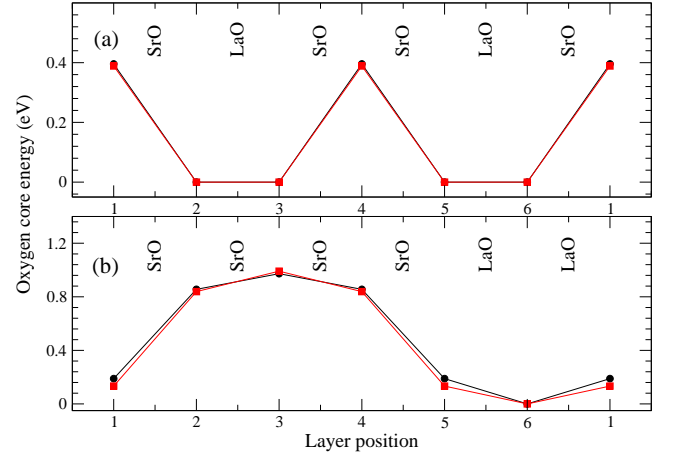


FIG. 8. (Color online). The variations of the relative oxygen $1s$ core energy (calculated using GGA) in each MnO_2 layer of (a) $\text{LaMnO}_3/(\text{SrMnO}_3)_2$ and (b) $(\text{LaMnO}_3)_2/(\text{SrMnO}_3)_4$ superlattices. Results for SrTiO_3 and LaAlO_3 substrates are indicated by black circles and red squares, respectively. The layer positions are indicated in Fig. 1 (a) and Fig. 2 (a).

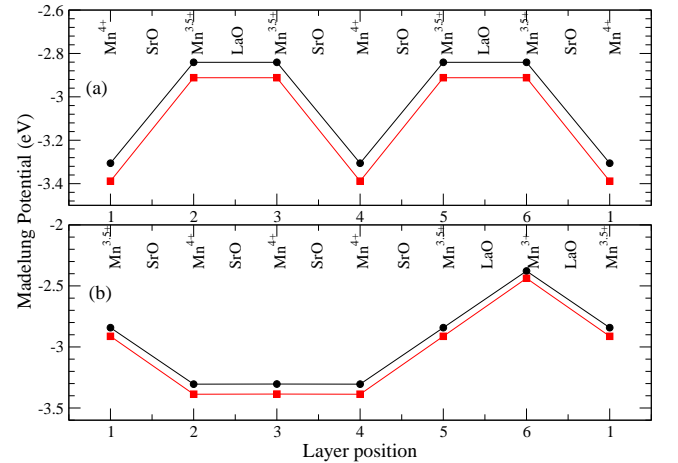


FIG. 9. (Color online). The variation of Madelung potential for Mn ions in each MnO_2 layer of (a) $\text{LaMnO}_3/(\text{SrMnO}_3)_2$ and (b) $(\text{LaMnO}_3)_2/(\text{SrMnO}_3)_4$ superlattices. Results for SrTiO_3 and LaAlO_3 substrates are indicated by black circles and red squares, respectively. Here, the ideal crystal structures with no distortion, and the ideal Mn valency (indicated in the figures) with O^{2-} , La^{3+} , and Sr^{2+} are assumed. The layer positions are indicated in Fig. 1 (a) and Fig. 2 (a). Note that the sign convention of Madelung potential used here is that electrons prefer to locate in LaMnO_3 layers.

IV. SUMMARY

Using first-principles calculations based on the density functional theory, we have studied the effects of epitaxial strain on the magnetic ground states in $(\text{LaMnO}_3)_n/(\text{SrMnO}_3)_{2n}$ (001) superlattices with $n = 1, 2$. Our results clearly demonstrate that as in alloy manganites, even in superlattices, the epitaxial strain induced by substrates enforces tetragonal distortion, which in turn governs the ground state magnetic structure via the inherent orbital ordering. We have found that for the tensile strain induced by SrTiO_3 (001) substrate, the ground state is A-type antiferromagnetic metal with $d_{x^2-y^2}$ orbital order. The approximate estimation of an effective magnetic exchange suggests that the Néel temperature T_N of the A-type antiferromagnetic order is higher for $n = 1$ than that for $n = 2$. These results are in excellent agreement with experimental observations.¹⁴ Furthermore, we have predicted that for the compressive

strain induced by LaAlO_3 (001) substrate, the ground state is C-type antiferromagnetic metal with $d_{3z^2-r^2}$ orbital order with higher Néel temperature T_N for $n = 1$ than that for $n = 2$. These predictions should be confirmed experimentally in the future.

ACKNOWLEDGMENTS

The computation is done using the RIKEN Integrated Cluster of Clusters (RICC). Q. Z. was supported by the Natural Science Foundation of Jiangsu Province (BK2012248), and research fund of Key Laboratory for Advanced Technology in Environmental Protection of Jiangsu Province (AE201152). S. D. was supported by the 973 Projects of China (2011CB922101), NSFC (11004027), and NCET (10-0325). B. W. was supported by NSFC (11174242).

-
- * qfangzhang@gmail.com
- ¹ M. Imada, A. Fujimori, and Y. Tokura, *Rev. Mod. Phys.* **70**, 1039 (1998).
 - ² C. H. Ahn, A. Bhattacharya, M. Di Ventura, J. N. Eckstein, C. D. Frisbie, M. E. Gershenson, A. M. Goldman, I. H. Inoue, J. Mannhart, A. J. Millis, A. F. Morpurgo, D. Natelson, and J. M. Triscone, *Rev. Mod. Phys.* **78**, 1185 (2006)
 - ³ A. Ohtomo and H. Y. Hwang, *Nature* **427**, 423 (2006).
 - ⁴ H. Y. Hwang, Y. Iwasa, M. Kawasaki, B. Keimer, N. Nagaosa, and Y. Tokura, *Nature Mater.* **11**, 103 (2012).
 - ⁵ E. Dagotto, T. Hotta, and A. Moreo, *Phys. Rep.* **344**, 1 (2001).
 - ⁶ C. Adamo, X. Ke, P. Schiffer, A. Soukiassian, M. Warusawithana, L. Maritato, and D. G. Schlom, *Appl. Phys. Lett.* **92**, 112508 (2008).
 - ⁷ H. B. Zhao, K. J. Smith, Y. Fan, G. Lüpke, A. Bhattacharya, S. D. Bader, M. Warusawithana, X. Zhai, and J. N. Eckstein, *Phys. Rev. Lett.* **100**, 117208 (2008).
 - ⁸ A. Bhattacharya, S. J. May, S. G. E. Te Velthuis, M. Warusawithana, X. Zhai, B. Jiang, J. Zuo, M. R. Fitzsimmons, S. D. Bader, and J. N. Eckstein, *Phys. Rev. Lett.* **100**, 257203 (2008).
 - ⁹ A. Perucchi, L. Baldassarre, A. Nucara, P. Calvani, C. Adamo, D. G. Schlom, P. Orgiani, L. Maritato, and S. Lupi, *Nano Lett.* **10**, 4819 (2010).
 - ¹⁰ A. Galdi, C. Aruta, P. Orgiani, C. Adamo, V. Bisogni, N. B. Brookes, G. Ghiringhelli, D. G. Schlom, P. Thakur, and L. Maritato, *Phys. Rev. B* **85**, 125129 (2012).
 - ¹¹ S. Dong, R. Yu, S. Yunoki, G. Alvarez, J.-M. Liu, and E. Dagotto, *Phys. Rev. B* **78**, 201102(R) (2008).
 - ¹² B. R. K. Nanda and S. Satpathy, *Phys. Rev. B* **79**, 054428 (2009).
 - ¹³ A. Bhattacharya, X. Zhai, M. Warusawithana, J. N. Eckstein, and S. D. Bader, *Appl. Phys. Lett.* **90**, 222503 (2007).
 - ¹⁴ S. J. May, P. J. Ryan, J. L. Robertson, J. Kim, T. S. Santos, E. Karapetrova, J. L. Zarestky, X. Zhai, S. G. E. Te Velthuis, J. N. Eckstein, S. D. Bader, and A. Bhattacharya, *Nature Mater.* **8**, 892 (2009).
 - ¹⁵ G. Kresse and J. Hafner, *Phys. Rev. B* **47**, 558 (1993).
 - ¹⁶ G. Kresse and J. Furthmüller, *Phys. Rev. B* **54**, 11169 (1996).
 - ¹⁷ P. E. Blöchl, *Phys. Rev. B* **50**, 17953 (1994).
 - ¹⁸ G. Kresse and D. Joubert, *Phys. Rev. B* **59**, 1758 (1999).
 - ¹⁹ S. L. Dudarev, G. A. Botton, S. Y. Savrasov, C. J. Humphreys, and A. P. Sutton, *Phys. Rev. B* **57**, 1505 (1998).
 - ²⁰ V. Anisimov, F. Aryasetiawan, and A. Lichtenstein, *J. Phys.: Condens. Matter* **9**, 767 (1997).
 - ²¹ P. E. Blöchl, O. Jepsen, and O. K. Andersen, *Phys. Rev. B* **49**, 16223 (1994).
 - ²² E. O. Wollan and W. C. Koehler, *Phys. Rev.* **100**, 545 (1955).
 - ²³ R. H. Mitchell, A. R. Chakhmouradian and P. M. Woodward, *Phys. Chem. Minerals* **27**, 583 (2000).
 - ²⁴ A. Nakatsuka, O. Ohtaka, H. Arima, N. Nakayama and T. Mizota, *Acta Crystallogr. E* **61**, 148 (2005).
 - ²⁵ Note that with the GGA+ U scheme a Stoner type ferromagnetic state is expected stable for large values of U_{eff} .
 - ²⁶ Z. Fang, I. V. Solovyev, and K. Terakura, *Phys. Rev. Lett.* **84**, 3169 (2000).